Direct observation of first-chance fission of ^{258}No

D. Peterson* and W. Loveland
Department of Chemistry, Oregon State University, Corvallis, Oregon 97331, USA

O. Batenkov, M. Majorov, and A. Veshikov
V. G. Khlopin Radium Institute, St. Petersburg, Russia

K. Aleklett and C. Rouki
Uppsala University, Uppsala, Sweden

(Received 9 June 2008; revised manuscript received 26 November 2008; published 27 April 2009)

The multiplicities, angular correlations, and energy spectra of the neutrons associated with fission were measured for the reactions of ^{25,26}Mg + ^{232}Th at ^{25}Mg and ^{26}Mg projectile energies of 132 and 148 MeV, respectively. From these data, we extracted a value of Γ_n/Γ_f for the first-chance fission of ^{258}No at an excitation energy of 61 MeV. The implications of this result for understanding the survival probabilities of excited heavy nuclei formed in "hot" fusion reactions are discussed.

DOI: 10.1103/PhysRevC.79.044607 PACS number(s): 25.70.Jj, 25.60.Pj, 25.85.−w, 27.90.+b

I. INTRODUCTION

Some of the more interesting questions in nuclear physics pertain to the production, stability, and structure of the heaviest elements. The methods employed in the synthesis of new heavy nuclei are influenced by, and enhance the present understanding of physics at, the limits of nuclear stability. Cold fusion reactions, where the excitation energies of the compound nucleus are relatively low ($E^* = 10$–15 MeV), permitting deexcitation by the emission of a single neutron, suffer from fusion hindrance that limits the cross sections. Conversely, hot fusion involving asymmetric reaction partners with actinide targets have small fusion hindrance, but the resultant excitation energies are so large ($E^* = 30$–60 MeV), that the survival of the product nucleus against fission becomes smaller. (For excited heavy nuclei, there is a competition between decay by fission and decay by neutron emission, with charged particle emission being suppressed by the high Coulomb barriers for such processes). This competition is expressed formally by the ratio of the widths for neutron emission and fission, $\frac{\Gamma_n}{\Gamma_f}$. The cross section for producing a heavy evaporation residue, σ_{EVR}, in a fusion reaction can be written as

$$\sigma_{\mathrm{EVR}} = \sum_{J=0}^{J_{\max}} \sigma_{\mathrm{capt.}}(E_{\mathrm{c.m.}}, J) P_{\mathrm{CN}}(E_{\mathrm{c.m.}}, J) W_{\mathrm{sur}}, \qquad (1)$$

where $\sigma_{\mathrm{capt.}}(E_{\mathrm{c.m.}}, J)$ is the capture cross section at center-of-mass energy $E_{\mathrm{c.m.}}$ and spin J. P_{CN} is the probability that the projectile-target system will evolve inside the fission saddle point to form a completely fused system rather than reseparating (quasifission). W_{sur} is the probability that the completely fused system will deexcite by neutron emission rather than fission. For a quantitative understanding of the synthesis of new heavy nuclei, one needs to understand $\sigma_{\mathrm{capt.}}$, P_{CN}, and W_{sur} for the reaction system under study.

The survival probability is given by $(\frac{\Gamma_n}{\Gamma_{\mathrm{tot}}})_i$ at each step i of the deexcitation chain, where $\frac{\Gamma_n}{\Gamma_{\mathrm{tot}}}$ equals $\frac{\Gamma_n}{\Gamma_n+\Gamma_f}$. For very heavy nuclei, frequently $\Gamma_f \gg \Gamma_n$ and $\frac{\Gamma_n}{\Gamma_{\mathrm{tot}}} \approx \frac{\Gamma_n}{\Gamma_f}$.

The published cross sections for the production of superheavy elements 113–118 [1] using hot fusion reactions with ^{48}Ca beams, as well as somewhat older data of Andreyev [2] involving the production of ^{258}No via hot fusion in the Mg + Th reaction, may indicate the presence of unexpected nuclear effects or physics, as understanding these data require unusually large values of $\frac{\Gamma_n}{\Gamma_f}$ compared to expectations from systematic trends. Sikkeland *et al.* [3] and Cherepanov *et al.* [4] have parametrized the average behavior of Γ_n/Γ_f for the No isotopes as well as several other transcurium nuclei. Using the systematics of Ref. [3], we would expect to find an average value of $\frac{\Gamma_n}{\Gamma_f} = 0.076$ for ^{258}No, while the parametrization of Ref. [4] gives $\frac{\Gamma_n}{\Gamma_f} = 0.056$ integrated over all chances to fission. Assuming that $\Gamma_{\mathrm{tot}} = \Gamma_n + \Gamma_f$ at these excitation energies, these values translate to $\frac{\Gamma_n}{\Gamma_{\mathrm{tot}}}$ values of 0.070 and 0.053, respectively, averaged over the entire deexcitation chain. These expectations are possibly at odds with the measurements of Ref. [2], in which the authors extracted a value of 0.8 for $\frac{\Gamma_n}{\Gamma_{\mathrm{tot}}}$, averaged over the first two steps only. In a previous attempt [5] to extract the first-chance fission probability, Loveland studied the evaporation residues from the ^{24,25,26}Mg + ^{232}Th reactions and found values of 0.058 and 0.065 for $\frac{\Gamma_n}{\Gamma_{\mathrm{tot}}}$ for the first and second steps in the deexcitation. These are also in stark disagreement with the results of Ref. [2].

In this work, we also study the Mg + Th reaction (at $E^* \approx 60$ MeV) utilizing cross bombardments with the intent of extracting the first-chance fission probability, and, hence, the primary value of $\frac{\Gamma_n}{\Gamma_f}$ in the first step of the deexcitation. However, the present measurement technique differs from the earlier measurements of Refs. [2,5] in that we directly

*Physics Division, Argonne National Laboratory, Argonne, Illinois, USA.

measure the neutrons emitted from the cooling compound system rather than measuring evaporation residue (EVR) cross sections. One advantage of this method is that the fission cross sections are many orders of magnitude larger than the EVR cross sections. It will also turn out (see below) that direct measurements of the emitted neutrons are more sensitive to the first steps in the deexcitation chain than evaporation residue measurements, which are most sensitive to the last steps in the deexcitation chain. The reaction studied also has two convenient features. First, the Z_1Z_2 product (1080) is small enough that one does not, in general, expect significant fusion hindrance or quasifission [6–8]. Second, the excitation energy (50–60 MeV) is high enough so that shell effects are expected to be washed out and unimportant [9,10] for the first members of the deexcitation chain. Regarding the first feature, it should be noted that Hinde *et al.* [11] observed events in the $^{32}S + ^{232}Th$ reaction ($Z_1Z_2 = 1440$) that they interpreted as quasifission events based, in part, on their angular distributions. (Note the caution of Samant and Kailas [12] regarding the interpretation of anomalous angular distributions for reactions involving deformed targets and the failure of Itkis *et al.* [13] to observe significant quasifission in the $^{48}Ca + ^{208}Pb$ reaction ($Z_1Z_2 = 1640$)). Thus it is not completely clear to what extent quasifission occurs in the $^{25,26}Mg + ^{232}Th$ reactions. Aritomo, Ohta, and Hanappe [14] have shown, however, that quasifission leads to smaller prescission-neutron multiplicities than fusion-fission, and the point of this manuscript is the large observed prefission neutron multiplicities.

Complementary to the technique of extracting the survival probability $\frac{\Gamma_n}{\Gamma_f}$ from EVR measurements, as performed in the studies cited above, one can measure the evaporated neutrons and the fission fragments to directly compare the decay widths. The key lies in understanding the complex neutron spectra as discussed below. In a fusion-fission reaction, there are several potential sources of neutrons including statistical evaporation from the compound system, preequilibrium emission from the interacting particles, each of the fully accelerated fission fragments, and possibly emission during the scission process itself. Harding and Farley [15] pioneered the technique of deconvoluting neutron spectra into an isotropic (compound system) and kinematically focussed (fission fragment) component in the mid-1950s. Since then, the technique has expanded to include the various other sources of neutron emission in a fissionable system; see, for example, Ref. [16]. If one assumes that neutron emission occurs isotropically in the rest frame of the emitting source, then emission from the equilibrated compound system will be characteristically isotropic in the laboratory frame (aside from a minor kinematic shift from the recoiling system), whereas neutrons emitted postfission from the fully accelerated fragments will be characteristically focused in the direction of the emitting fragment, with higher energies due to the kinematic boost given by the fragment's motion. Neutrons emitted during the scission process are emitted perpendicular to the plane of the fragments. This component is generally found to be small (about 0–20% of the total postfission neutron multiplicity) in these reactions; for a review of this subject, see Ref. [17]. Preequilibrium neutrons are similar to those emitted from the accelerated fragments, but they are focused in the beam direction with a source velocity on the order of 50% the beam velocity [18].

II. EXPERIMENTAL TECHNIQUE

A. Setup and design

The ^{26}Mg bombarding energy was chosen to match the measurements of Ref. [2]. In the reaction $^{26}Mg + ^{232}Th$, we detected neutrons from the decay chain

$$\begin{aligned} &^{258}\mathrm{No} \rightarrow {}^{257}\mathrm{No} \rightarrow {}^{256}\mathrm{No} \rightarrow {}^{255}\mathrm{No} \rightarrow {}^{254}\mathrm{No} \\ &\quad \rightarrow {}^{253}\mathrm{No} \rightarrow {}^{252}\mathrm{No}. \\ &E^*(\mathrm{MeV}) = 61 \rightarrow 51 \rightarrow 41 \rightarrow 31 \rightarrow 21 \rightarrow 10 \rightarrow 2 \end{aligned}$$

For the $^{25}Mg + ^{232}Th$ reaction, the bombarding energy was chosen such that its decay chain

$$\begin{aligned} &^{257}\mathrm{No} \rightarrow {}^{256}\mathrm{No} \rightarrow {}^{255}\mathrm{No} \rightarrow {}^{254}\mathrm{No} \\ &\quad \rightarrow {}^{253}\mathrm{No} \rightarrow {}^{252}\mathrm{No} \\ &E^*(\mathrm{MeV}) = 51 \rightarrow 41 \rightarrow 31 \rightarrow 21 \rightarrow 10 \rightarrow 2 \end{aligned}$$

energetically matches the corresponding elements of the ^{258}No chain, allowing a direct comparison of the neutrons emitted solely from that nucleus and avoiding the difficulties inherent in other, model-dependent analysis methods.

One may wonder whether the technique of cross bombardments actually allows us to deduce the properties of the first members of the deexcitation chains, since we expect differences in the spin distributions of the products formed in these reactions. To evaluate these differences, we used the same standard statistical model, HIVAP [19], to calculate and compare the excitation energy and spin distributions of ^{257}No formed directly in the $^{25}Mg + ^{232}Th$ reaction ($E^*_{av} = 51.1$ MeV and $J_{av} = 29.1 \pm 13.9\hbar$) as well as that formed after evaporating a neutron in the $^{26}Mg + ^{232}Th$ reaction ($E^*_{av} = 51.1$ MeV and $J_{av} = 35.7 \pm 17.2\hbar$). As a further test of this effect, we employed the same model to calculate the expected final product yields in these reactions. Using a set of standard "heavy element" input parameters [20], we calculated

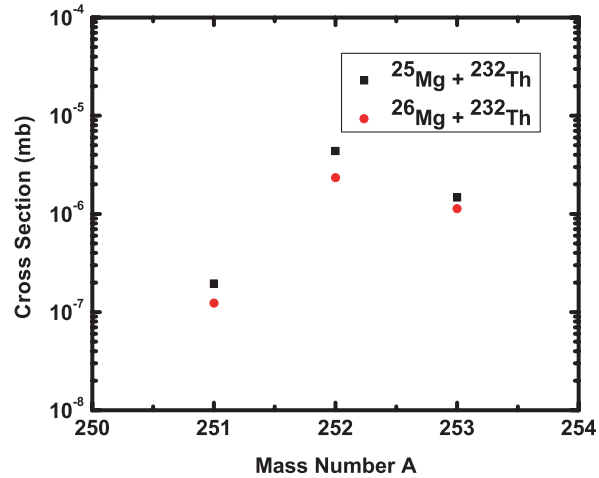

FIG. 1. (Color online) Calculated final product distributions in the reaction of 132 MeV ^{25}Mg and 148 MeV ^{26}Mg with ^{232}Th.

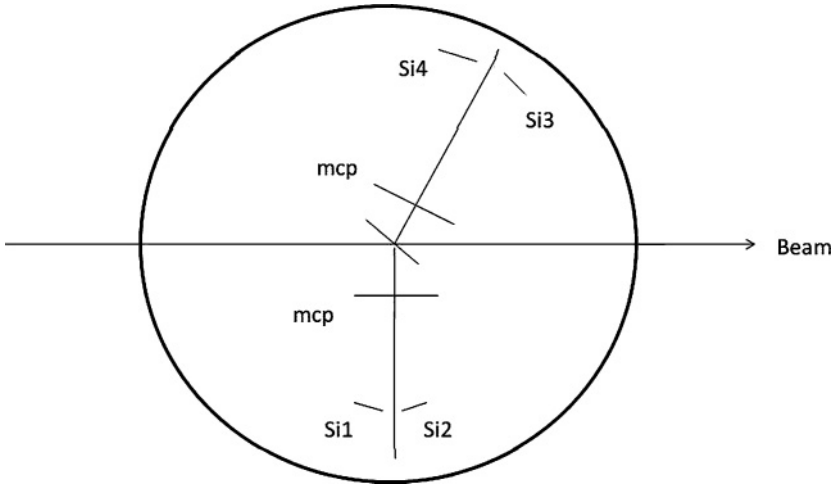

FIG. 2. (Color online) Schematic arrangement of the Si fission fragment detectors inside the thin-walled target chamber.

the final product yields in these two reactions with the same projectile energies used in this work (Fig. 1). The resulting calculated distributions for the two reactions are similar, indicating that the fission-neutron emission competition in the two reactions is expected to be similar.

The Mg beams were accelerated by the Gustaf Werner synchrocyclotron, located in Uppsala, Sweden, to energies of 149.3 (^{26}Mg) and 134.4 (^{25}Mg) MeV. These resulted in center-of-target reaction energies of 148.0 and 132.0 MeV, respectively. The thorium targets were configured in a back-to-back double sandwich consisting of 50 μg/cm^2 of Al_2O_3, 180 of Th, and 30 of Au, followed by 30 μg/cm^2 of Au, 140 of Th, and 50 of Al_2O_3. The target was tilted 45° with respect to the beam axis. The ^{232}Th targets were 99.99% ^{232}Th, with no significant heavy element impurities. Fission fragments were detected in four Si detectors of 1000 μm thickness and diameters of either 18 or 15 mm positioned at either 10.1 or 10.5 cm from the target at the folding angle for full momentum transfer. The solid angle for detecting a fission coincidence was 12.4 or 17.0 msr, depending on which Si pair was hit. Each fission fragment passed through an Al_2O_3 foil (thickness 60 μg/cm^2) mounted near the target. Delta electrons knocked out of this foil were accelerated by a short electrostatic field (2–5 kV) and struck a position sensitive microchannel plate detector, providing timing information. The experimental setup is illustrated in Fig. 2.

Neutrons were detected in coincidence with fission by an array of 11 stilbene crystals arranged in three orthogonal planes outside the reaction chamber at approximately 50 cm from the target. The total solid angle for neutron detection was slightly more than 1% of 4π. The detector arrangement is depicted in the diagrams of Fig. 3 and summarized in Table I.

Neutron time of flight (TOF) spectra were obtained from the time difference between a signal from one of the microchannel plate (MCP) detectors located near the target and a signal from the stilbene crystal. Fragment TOFs were obtained from the time difference between a MCP and Si detector. Neutron and γ-ray events in the detectors were separated by means of pulse shape discrimination in the off-line analysis. The setup used in this experiment was similar to that used in previously reported studies [21–23], and the reader is referred to those reports for a more complete description of the apparatus. An event was defined as a three-fold coincidence between a neutron detector and a MCP-Si pair. Random correlations in the neutron-MCP1-MCP2-Si12-Si34 trigger events were negligible. Such random events can be identified in the neutron TOF spectra.

B. Calibration and efficiencies

The efficiencies of the neutron detectors were obtained using a ^{252}Cf fission source placed at the target location. This source was mounted in a thin-walled, hemispherical (2π) ionization chamber that was nearly 100% efficient for detecting one of the two fission fragments, allowing us to normalize the number of detected neutrons to fissions. The neutron reference spectrum of Mannhart [24] was used in determining the energy dependence of the efficiencies. Efficiency measurements were made before and after the bombardments and then averaged. A typical efficiency curve for the stilbene detectors is shown as the solid squares in Fig. 4. The largest source of systematic error in this experiment comes from the efficiency, with uncertainties approaching 20% at energies above 8 MeV. In Fig. 4, we also compare this measured efficiency function with those of other measurements of similar stilbene detectors [21,22] and a simulated efficiency curve for

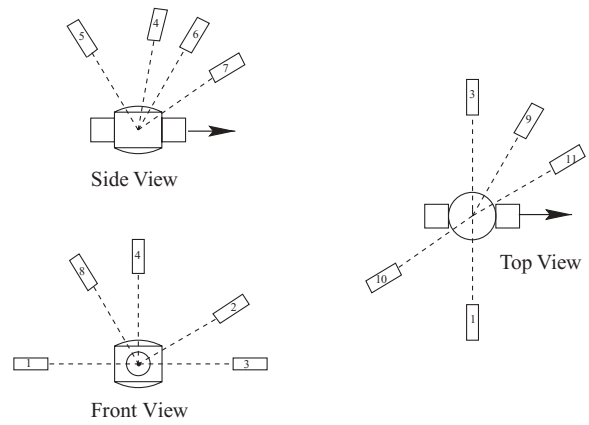

FIG. 3. Schematic diagram of the locations of the neutron detectors as described in Table I. The beam direction is indicated by the bold arrow.

TABLE I. Locations of neutron detectors. The crystal faces (diameter D) were located a distance d from the target. ϕ is measured counterclockwise from the beam direction, in the reaction plane defined by the beam and fragment detectors. θ measures the elevation above the reaction plane.

Detector no.	Detector D (cm)	^{25}Mg run			^{26}Mg run		
		d (cm)	ϕ (deg)	θ (deg)	d (cm)	ϕ (deg)	θ (deg)
1	7.0	47.5	270.0	0.0	270.0	0.0	48.4
2	6.3	49.8	90.0	34.2	90.0	34.0	49.1
3	7.0	47.2	90.0	0.0	90.0	0.0	47.6
4	7.0	48.4	0.0	77.3	0.0	79.7	48.6
5	5.0	47.2	0.0	120.0	0.0	120.5	47.3
6	5.0	47.4	0.0	58.8	0.0	59.6	47.5
7	5.0	50.6	0.0	33.7	0.0	33.9	50.0
8	5.0	48.9	270.0	55.3	270.0	54.3	50.1
9	5.0	49.3	59.5	0.0	59.1	0.0	48.0
10	5.0	48.4	215.1	0.0	216.7	0.0	41.3
11	7.0	48.9	33.5	0.0	35.6	0.0	47.3

these detectors [21], where the neutron detection threshold was 0.21 MeV.

Fragment energies were obtained directly from the surface barrier detectors, which were calibrated to account for effects of pulse-height defects. [25]. Even though time-of-flight information was available for the fragment detectors, fragment masses were obtained using momentum conservation. Neutron energies were determined from their measured TOFs. Some systematics of the measured quantities are shown in Figs. 5–7. Figures 5 and 6 illustrate the energy response (in the laboratory frame) and the deduced mass distributions for fragments entering the Si4 detector. Figure 7 depicts a typical TOF neutron spectrum and illustrates the effect of applying pulse-height discrimination to eliminate the prompt γ rays from our data. Examining the γ peak reveals a full width at half maximum (FWHM) resolution of 2 ns for the stilbene detectors. Finally, we show in Fig. 8 sample spectra (data points) for neutrons detected at 10° (our most forward angle) and 85° (our angle nearest 90°) relative to fragments incident to detector Si4. These can be compared with what one expects for neutrons emitted at 0°, 90°, and 180° relative to a 1.6 MeV source moving at a velocity of 0.80 cm/ns as shown in Fig. 8. (These are the mean temperature and velocity as determined from the complete analysis described below.)

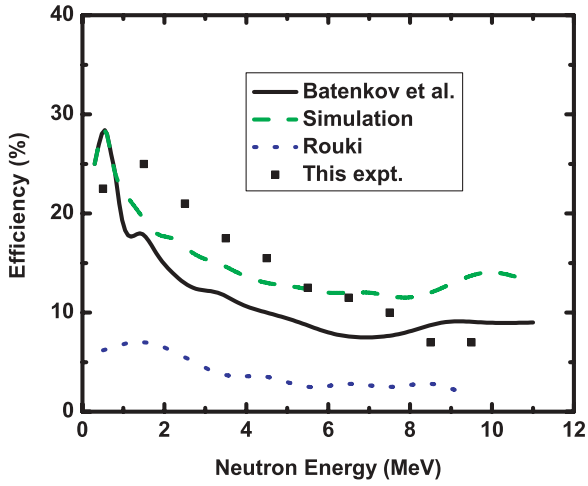

FIG. 4. (Color online) Comparison of typical stilbene efficiency as measured in the present experiment (squares) with previous measurements [21] (solid line) and [22] (dotted line) of similar stilbene detectors and a simulated response curve [21] (dashed line) for these detectors.

III. DYNAMIC SYSTEMATICS

A. Neutron emission in systems undergoing multiple chance fission

To help understand the issues involved in analyzing neutron emission in multiple-chance fission, consider the data in Table II. In Table II, we simulate the deexcitation of 1000 ^{258}No nuclei excited to an excitation energy $E*$ of 61 MeV using an arbitrary but reasonable set of assumptions about $\Gamma_n/\Gamma_{\rm tot}$ (see below). We have also assumed that the number

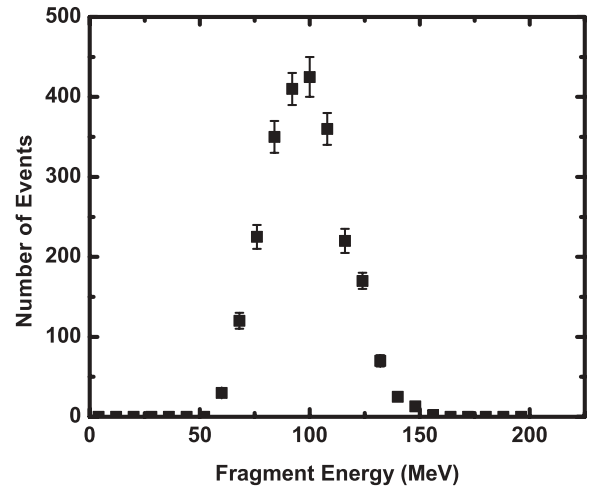

FIG. 5. Typical energy distribution for fission fragments detected in one of the silicon detectors.

TABLE II. Simulated deexcitation of ^{258}No.

Nucleus	^{258}No	^{257}No	^{256}No	^{255}No	^{254}No	^{253}No	^{252}No
E^* (MeV)	61	51	41	31	21	10	2
No. nuclei	1000	250	90	11	2.3		
$\Gamma_n/\Gamma_{\rm tot}$	0.25	0.36	0.12	0.21	0.013	0.0056	
No. of fissions	750	160	79	8.7	2.3		
$\nu_{\rm post}$	4.2	4.2	4.2	4.2	4.2	4.2	
No. postfission neutrons	3150	672	332	36.5	9.7		
No. prefission neutrons	250	90	11	2.3			

of postfission neutrons emitted per fission, $\nu_{\rm post}$, is the same for each member of the chain and have set that value at 4.2, which is the value of $\nu_{\rm post}$ found for the spontaneous fission of ^{252}No [26]. One observes that in this simulation, most of the neutrons are emitted in the early stages of the deexcitation process, but the largest effects on the final product yields occur at the end of the deexcitation chains, where $\Gamma_n/\Gamma_{\rm tot}$ is small, in this example. (We have neglected the effect of scission neutrons in this example [27,28]).

Averaged over the chain, $\Gamma_n/\Gamma_{\rm tot}$ is 0.11, while the average $\Gamma_n/\Gamma_{\rm tot}$ for the first two members of the chain is 0.3. The total number of prefission neutrons is 353, while the total number of postfission neutrons is ∼4200. Defining $^{258}\overline{\nu}_{\rm pre}$ and $^{257}\overline{\nu}_{\rm pre}$ as the average number of prefission neutrons emitted in the deexcitation of ^{258}No and ^{257}No, respectively, we can write

$$^{258}\overline{\nu}_{\rm pre} = \left(\frac{\Gamma_n}{\Gamma_{\rm tot}}\right)_1 + \left(\frac{\Gamma_n}{\Gamma_{\rm tot}}\right)_1\left(\frac{\Gamma_n}{\Gamma_{\rm tot}}\right)_2 + \left(\frac{\Gamma_n}{\Gamma_{\rm tot}}\right)_1\left(\frac{\Gamma_n}{\Gamma_{\rm tot}}\right)_2\left(\frac{\Gamma_n}{\Gamma_{\rm tot}}\right)_3 + \cdots, \quad (2)$$

$$^{257}\overline{\nu}_{\rm pre} = \left(\frac{\Gamma_n}{\Gamma_{\rm tot}}\right)'_1 + \left(\frac{\Gamma_n}{\Gamma_{\rm tot}}\right)'_1\left(\frac{\Gamma_n}{\Gamma_{\rm tot}}\right)'_2 + \left(\frac{\Gamma_n}{\Gamma_{\rm tot}}\right)'_1\left(\frac{\Gamma_n}{\Gamma_{\rm tot}}\right)'_2\left(\frac{\Gamma_n}{\Gamma_{\rm tot}}\right)'_3 + \cdots. \quad (3)$$

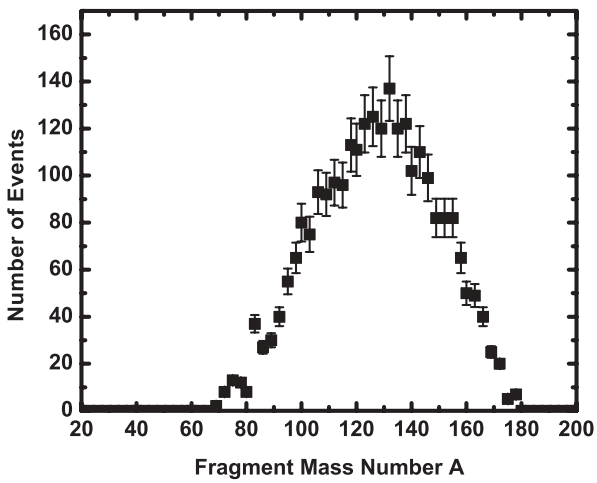

FIG. 6. Typical mass distribution for fission fragments detected in one of the silicon detectors.

Recognizing that $(\frac{\Gamma_n}{\Gamma_{\rm tot}})'_1$ is the same as $(\frac{\Gamma_n}{\Gamma_{\rm tot}})_2$, the above equations yield a simple result for determining the survival probability for the first-chance fission of ^{258}No:

$$\left(\frac{\Gamma_n}{\Gamma_{\rm tot}}\right)_1 = \frac{^{258}\overline{\nu}_{\rm pre}}{1 + {}^{257}\overline{\nu}_{\rm pre}}. \quad (4)$$

Decomposing the neutron spectra to extract the isotropic component leads to a simple and straightforward method of determining the first-chance fission probability.

B. Isolating the isotropic component

Prefission neutrons are emitted isotropically in the laboratory system (aside from the small boost from the recoiling compound nucleus), whereas neutrons emitted from fission fragments are strongly correlated with the fission direction of motion in the laboratory frame. For this reason, neutrons are typically measured at 0° and 90° relative to the fragment motion. However, our setup configuration limited our neutron-fragment correlation angles to the range of 10°–85°. Since correlation (or lack thereof) with fragment motion is imperative to the determination of a detected neutron's source, only events in which a fission-fragment pair was detected were considered in the analysis. Typical fragment spectra from this experiment are shown in Figs. 5 and 6, and neutron spectra appear in Fig. 7.

The complete analysis presented in this paper involved performing a multicomponent, moving-source fit to all neutron spectra. We considered neutrons emitted from four sources: (1) the recoiling compound nucleus (CN), (2) the primary fragment (PF), whose direction is most strongly correlated with that of the neutron, (3) the complementary fragment (CF), and (4) preequilibrium (PQ) processes where the neutrons are emitted immediately from the reacting system rather than as from a well-defined system such as a fragment or the compound nucleus. Neutrons emitted from the neck at the moment of scission were not explicitly treated but are considered, for the purposes of our analysis, as part of the postfission neutrons. By fitting all 11 spectra simultaneously, we could achieve a best fit for the number of neutrons emitted per fission event from any given source. This allows us to obtain better numbers for pre- and postfission neutron numbers. The fitting routine also properly accounts for the Jacobian transformations among the various moving source frames to maintain properly normalized solid angles for detection. Aside from the three multiplicities, the temperature

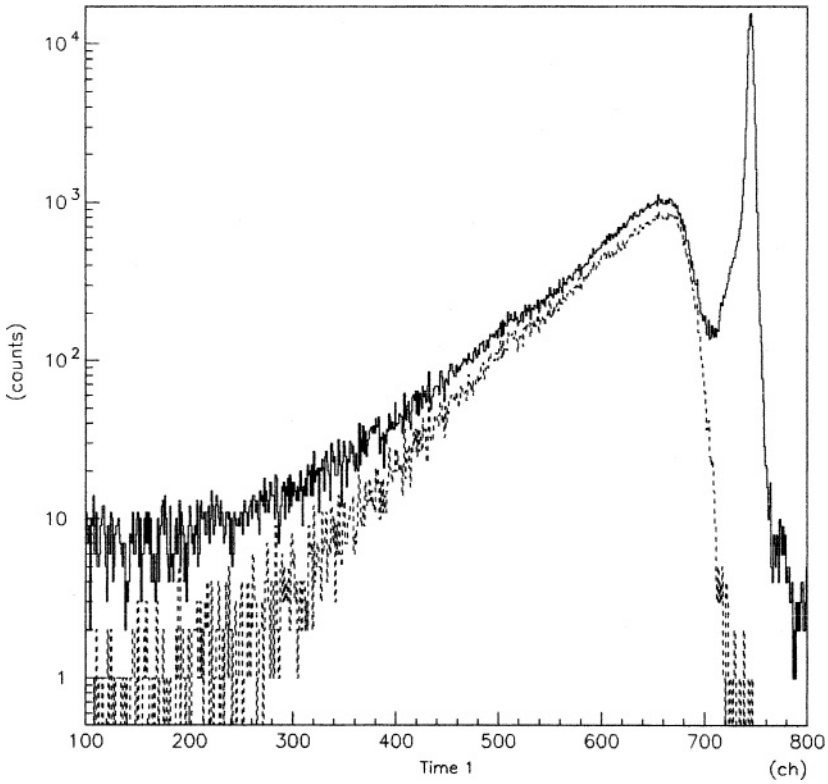

FIG. 7. Time-of-flight for one of the neutron detectors illustrating the ability to discriminate via pulse-height methods. The full histogram constitutes all events in this detector. The dotted line represents the events determined to be "neutrons" rather than γ's by comparing the prompt and full pulse heights.

of the emitting sources are also allowed to vary. However, the velocities of the sources are held fixed to the mean velocities measured in the Si surface barrier (SSB) detectors.

IV. RESULTS

A. Expectations from simple models

To obtain a feeling for what can be expected in each spectrum, one can refer to Fig. 8. Here, we have simulated a fragment in motion with the mean velocity measured for the fragments in this experiment and isotropically ejected 10^8 neutrons from a Maxwellian distribution corresponding to a temperature of 1.6 MeV. We then examined the energy distribution that would be observed in 2° cones centered at 0°, 90°, and 180°. From this figure, it is clear that the contribution from the complementary fragment is very small because of the center-of-momentum motion. This figure also illustrates the basic relationship between energy and angle for the neutrons. That is, when neutrons are emitted in the fragment direction they gain a kinematic boost from the fragment's motion, shifting their energies higher. This also has an effect of forward-focusing the distribution, effectively increasing the solid angle of the forward neutron detector. As one moves backward in angle, the peak energy shifts to lower energies as the kinematic gain transitions to a kinematic loss. Consequently, the Jacobian transform also reduces the effective solid angle for these backward detectors.

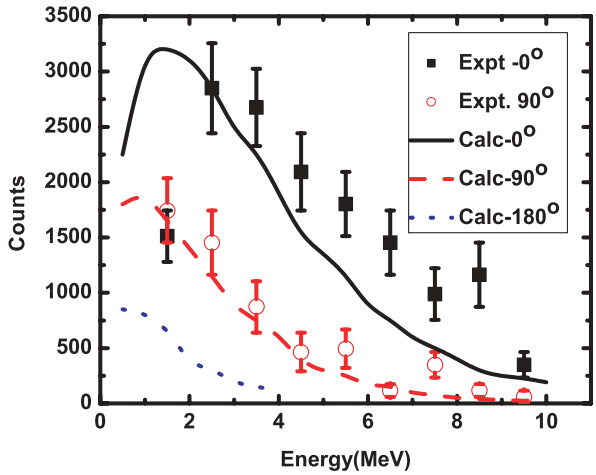

FIG. 8. (Color online) Comparison of neutron energy spectra for neutrons emitted at 0°, 90°, and 180° relative to a fragment moving with velocity 0.8 cm/ns. See text for details.

B. Observations

The results for the decomposition fits are presented in Figs. 9–11. The parameters extracted from these fits are summarized in Table III. In all plots, the solid black line is the total fit, the green and blue dashed lines are the components due to the fragment collected in the SSB detectors on either side of the target, and the dotted red line represents the contribution from the compound system (prefission) to the total neutron spectrum. Error bars on the data represent statistical and systematic errors, summed in quadrature. The data are plotted as counts/MeV msr vs neutron energy. The relative angles between the fission detector and the corresponding component for each detector pair is also provided in each panel. The preequilibrium component was found to be zero in each case and is not shown in the plots or summarized in Table III.

TABLE III. Multiplicities for neutrons originating from the equilibrated compound nucleus (CN), and the two fragments (FF1, FF2) for each of the fits performed in this analysis. Uncertainties were determined by examining the χ^2 parameter space. In addition to the neutron multiplicity decomposition, we also list the total number of fission coincidences registered for each set, the degrees of freedom (dof), the reduced χ^2 for the fits, and the CN temperature (in MeV) obtained in the fit.

	^{26}Mg	^{25}Mg	
	50–100 pair	50–100 pair	70–80 pair
CN	3.95 ± 0.19	3.43 ± 0.27	3.95 ± 0.20
FF1	4.81 ± 0.15	3.59 ± 0.15	3.18 ± 0.11
FF2	3.76 ± 0.19	2.38 ± 0.19	2.34 ± 0.17
Coincidences	191 219	126 807	178 444
dof	85	95	71
χ^2_ν	1.74	1.57	1.56
$T_{\rm CN}$ (MeV)	1.60	1.48	1.48

During the ^{26}Mg irradiation, one of the SSB detectors was shadowed by the target ladder, causing the coincidences from that corresponding pair to be essentially nonexistent. Therefore, we only have one set of data to fit for the ^{258}No decay. However, this problem was fixed for the ^{25}Mg bombardment, and we could obtain measurements for both fission detector pairs. We find a consistent decomposition of the neutron spectrum for both pairs, as seen in Table III. In examining Figs. 9–11, a few features are worth pointing out. We find that, as expected, for detectors most closely aligned with the fragment direction, the strongest component is from that fragment with very little contribution from the

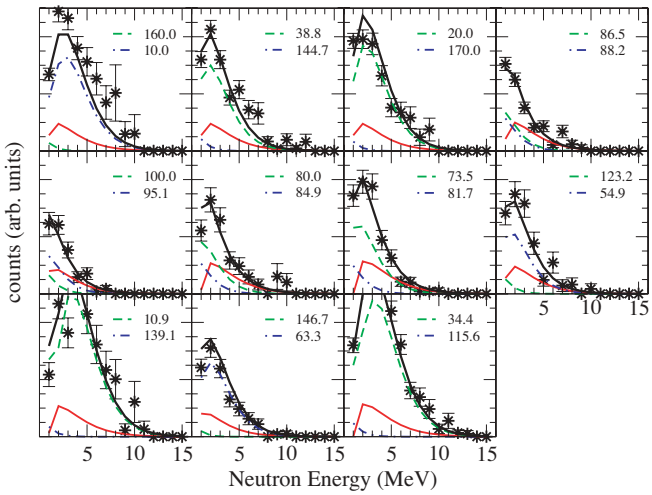

FIG. 9. (Color online) Results of the three-source fit to the ^{26}Mg bombardment data for fission detector pair 1–3 (as labeled in Fig. 2). The contribution from compound nucleus (prefission) neutrons is shown by the thin solid (red) line. The dashed (blue) and dot-dashed (green) lines illustrate the contributions from postfission neutrons emitted from the fragment hitting the beam-left and beam-right detectors. The thick black line shows the total spectrum. The angles between the fragment and neutron detectors are listed in each panel.

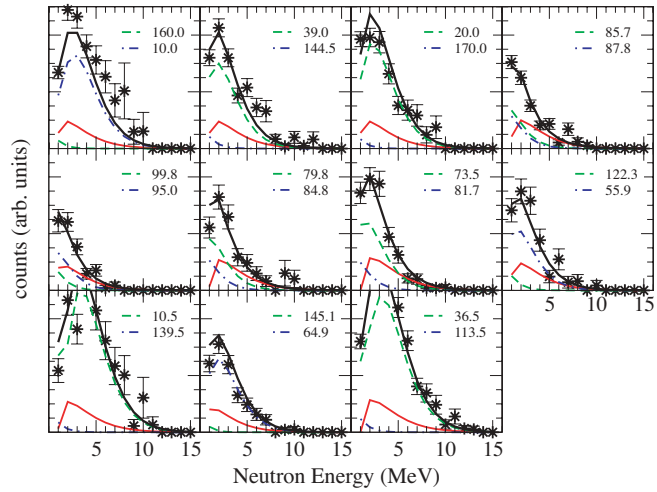

FIG. 10. (Color online) Results of the three-source fit to the ^{25}Mg bombardment data for fission detector pair 1–3 (as labeled in Fig. 2). Lines have the same meaning as in Fig. 9.

complementary fragment. For the detectors near 90°, both detectors receive nearly identical contributions from either fragment. We also notice that the only source for neutrons with energies above 8 MeV is collinear emission from a fragment, and that the CN (isotropic) component contributes mainly to the low-energy region.

From the values listed in Table III and the use of Eq. (2), we obtain (using the weighted average of the two ^{25}Mg fits) a value of 0.840 ± 0.050 for the first-chance $\frac{\Gamma_n}{\Gamma_{\rm tot}}$. This implies 5.27 ± 1.95 for first-chance $\frac{\Gamma_n}{\Gamma_f}$. The measured value of $\frac{\Gamma_n}{\Gamma_{\rm tot}}$ of 0.840 ± 0.050 for ^{258}No can be compared with other similar measurements. Andreyev *et al.* [2] deduced a value of $\frac{\Gamma_n}{\Gamma_{\rm tot}}$ of 0.8 averaged over the first two members of the deexcitation chain for this reaction. (In a previous measurement [29], they found $\frac{\Gamma_n}{\Gamma_{\rm tot}} = 0.30 \pm 0.15$ for this same quantity.) Simbel [30] deduced a value of $\frac{\Gamma_n}{\Gamma_{\rm tot}} = 0.081$ for ^{258}No ($E^* = 51$ MeV)

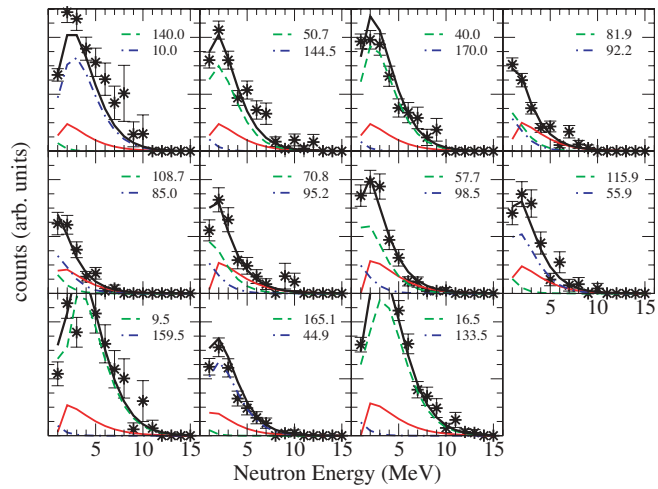

FIG. 11. (Color online) Results of the three source fit to the ^{25}Mg bombardment data for fission detector pair 2–4 (as labeled in Fig. 2). Lines have the same meaning as in Fig. 9.

TABLE IV. Parameters used in calculating $\Gamma_n/\Gamma_{\rm tot}$.

Nucleus	^{258}No	^{257}No	^{256}No	^{255}No	^{254}No	^{253}No
E^* (MeV)	61	51	41	31	21	10
B_n (MeV)	6.81	5.66	7.10	5.94	7.81	6.49
$U_{\rm shell}$ (MeV) (MNMS)	3.57	4.11	4.19	4.44	4.65	4.49
Damped $U_{\rm shell}$ (MeV)	0.43	0.70	0.98	1.41	2.24	3.17
$B_f^{\rm total}$ (MeV) (MNMS)	0.87	1.13	1.39	1.82	2.63	3.55
$\Gamma_n/\Gamma_{\rm tot}$ (MNMS)	0.25	0.36	0.12	0.21	0.013	0.0056
$U_{\rm shell}$ (MeV) (Cwiok)	5.46	5.37	5.99	6.00	6.71	7.32
$\Gamma_n/\Gamma_{\rm tot}$ (Cwiok)	0.28	0.39	0.16	0.28	0.04	0.26
$\Gamma_n/\Gamma_{\rm tot}$ (Kramers)	0.74	0.80	0.44	0.54	0.013	0.0056

but did show values ranging from 0.05 to 0.10 for various No nuclei excited with $E^* = 40$–50 MeV. As described earlier, Sikkeland *et al.* [3] and Cherepanov *et al.* [4] gave $\frac{\Gamma_n}{\Gamma_{\rm tot}}$ values of 0.076 and 0.056, respectively, (averaged over the deexcitation chain) for ^{258}No. The large discrepancy between the various measured values is disturbing, although the value deduced in this work is the only value obtained from a direct measurement of the neutrons associated with fission.

V. INTERPRETATION

To simulate in a simple and transparent manner the neutron emission process in multiple-chance fission, one starts at the excitation energy E^* of the completely fused system and reduces it for each evaporation step by the binding energy of the emitted neutron and an assumed neutron kinetic energy of $2T$, where $T[=(E^*/a)^{1/2}]$ is the temperature of the emitting system. For calculating Γ_n/Γ_f, one uses the classical formalism from Vandenbosch and Huizenga [31]

$$\frac{\Gamma_n}{\Gamma_f} = \frac{4A^{2/3}a_f(E^*-B_n)}{ka_n\left[2a_f^{1/2}(E^*-B_f)^{1/2}-1\right]} \times \exp\left[2a_n^{1/2}(E^*-B_n)^{1/2}-2a_f^{1/2}(E^*-B_f)^{1/2}\right], \quad (5)$$

where a_f and a_n are the level density parameters at the saddle point and the equilibrium deformation. The constant k is taken to be 9.8 MeV, and $a_n = a_f = A/12$. The fission barriers B_f are written as the sum of liquid drop $B_f^{\rm LD}$ and shell correction terms as

$$B_f(E^*_{\rm CN}) = B_f^{\rm LD} + U_{\rm shell}\exp[-\gamma E^*], \quad (6)$$

where

$$\gamma^{-1} = 5.48A^{1/3}/(1+1.3A^{-1/3})\ {\rm MeV}, \quad (7)$$

where the shell correction energies, $U_{\rm shell}$, to the LDM barriers are taken from Ref. [32], the liquid drop barriers are taken from Ref. [33], and the fadeout of the shell corrections with increasing excitation energy are taken from Ignatyuk *et al.* [34]. (We ignore shell effects on the saddle point [35].) Neutron binding energies B_n are taken from Ref. [32]. Collective enhancement effects are only important for spherical product nuclei and should have an insignificant effect on axially deformed nuclei such as the No isotopes where $\beta_2 \sim 0.2$ [7]. This simple formalism should have the virtue of allowing one to understand the physical factors that affect the survival probabilities.

The results of using this simple formalism, termed MNMS (Moller, Nix, Myers, Swiatecki), to calculate $\frac{\Gamma_n}{\Gamma_{\rm tot}}$ are given in Table IV along with the parameters used in the calculation. The dominant effect in the calculation is the fadeout of the ground state shell correction with increasing excitation energy, which leads to a calculated value of $\frac{\Gamma_n}{\Gamma_{\rm tot}}$ of 0.25 rather than the measured value of 0.840 ± 0.050. One does note the geometric mean of the calculated $\frac{\Gamma_n}{\Gamma_{\rm tot}}$ values is 0.074, which is similar to the values deduced from evaporation residue measurements [3,4]. One is then led to inquire whether a different set of assumptions/input parameters would lead to a different conclusion or a calculated value of $\frac{\Gamma_n}{\Gamma_{\rm tot}}$ that is closer to the measured value. The values of the neutron binding energies were taken from Ref. [32] for consistency with the fission barrier heights used [32]. But the MNMS B_n values are very similar to the known values of B_n [36], and thus this quantity is not the source of the disagreement.

What about the fission barrier heights? Cwiok *et al.* [37] have computed a rather different set of values of the fission barrier heights (and the shell effects deduced from them by subtracting the liquid drop barriers from the calculated fission barriers). These values are tabulated in Table IV (labeled Cwiok) along with the values of $\frac{\Gamma_n}{\Gamma_{\rm tot}}$ calculated from them. The calculated value of $\frac{\Gamma_n}{\Gamma_{\rm tot}}$ for ^{258}No excited to 61 MeV is 0.28 instead of the 0.25 value obtained with the Moller *et al.* [32] barriers. Even though the shell correction energies increased from 3.57 MeV to 5.46 MeV, the effect on $\frac{\Gamma_n}{\Gamma_{\rm tot}}$ was very small. In hot fusion reactions, such as the ones studied in this work, the survival probabilities at high excitation energies are not very sensitive to the values of the ground state fission barrier heights due to the fadeout of the shell correction energies. However, the final evaporation residue yields are sensitive to these quantities, as shown by taking the product of the $(\frac{\Gamma_n}{\Gamma_{\rm tot}})_i$ terms, which is 1.6×10^{-7} for the MNMS barriers and 5.0×10^{-5} for the Cwiok barriers.

In the formalism we have used, we set $a_f = a_n$ where a_f and a_n are the level density parameters for the fission saddle point and the ground state, respectively. To cause $\frac{\Gamma_n}{\Gamma_{\rm tot}}$ for ^{258}No ($E^* = 61$ MeV) to be 0.84 would require $a_f/a_n = 0.925$. This value of a_f/a_n is much lower than one observes in intermediate energy fission [38,39] and is inconsistent with

the general expectation [40,41] that the level density parameter will increase with deformation.

The situation we have is that of observing too many prescission neutrons compared to our simple statistical model calculations. The explanation for this effect was put forth by Kramers shortly after the discovery of fission [42]. Kramers pointed out that the nuclear viscosity would retard fission. Using this Kramers model for the dissipation, we can write [43] that

$$\Gamma_f = \Gamma_f^{BW}(\sqrt{1-x^2} - x) \times \hbar\omega_B/T, \tag{8}$$

where Γ_f is the corrected fission width, Γ_f^{BW} is the standard statistical model width for fission, x is the dimensionless dissipation coefficient where $x = \eta/2\omega_0$, where η is the nuclear viscosity, and ω_0 and ω_B are the characteristic frequencies of parabolic approximations of the nuclear potential energy near the ground state and the saddle point. B_f is the fission barrier height and T is the temperature. This approach is discussed in further detail in Refs. [44–46]. A value of $\Gamma_n/\Gamma_{\rm tot}$ of 0.74 for ^{258}No ($E^* = 61$ MeV) is predicted, and the geometric mean of the $\frac{\Gamma_n}{\Gamma_{\rm tot}}$ values over the deexcitation chain is 0.15.

VI. CONCLUSIONS

What have we learned from this study? We can make the following conclusions:

(i) For hot fusion reactions such as those studied in this work, the ground state fission barrier heights have a small influence on the survival probabilities in the first steps of the deexcitation process but are important for the overall survival probability.

(ii) The measurement of the prescission neutrons in hot fusion reactions is a more direct, sensitive way of determining the survival probabilities in the initial stages of the deexcitation process.

(iii) The values of $\nu_{\rm pre}$ and $\frac{\Gamma_n}{\Gamma_{\rm tot}}$ for the first-chance fission of hot actinide nuclei can be understood quantitatively in terms of modern calculations of survival probabilities.

(iv) For the particular system under study, ^{258}No ($E^* = 61$ MeV), the best values of $\frac{\Gamma_n}{\Gamma_{\rm tot}}$ for first-chance fission are $\sim$0.8, which is an order of magnitude larger than the values that have been deduced from evaporation residue measurements.

ACKNOWLEDGMENTS

We appreciate the assistance of the Uppsala University cyclotron operations staff, particularly D. Wessman and D. Van Rooyen for providing the ^{25,26}Mg beams. We also thank J. P. Lestone of Los Alamos for helpful discussions in interpreting the data. This work was supported in part under US Department of Energy Grant No. DE-FG06-97ER 41026 and funds from the Swedish Research Council.

[1] Y. T. Oganessian, J. Phys. G: Nucl. Part. Phys. **34**, R165 (2007).
[2] A. N. Andreyev, D. D. Bogdanov, V. I. Chepegin, A. P. Kabachenko, O. N. Malyshev, R. N. Sagaidak, L. I. Salamatin, G. M. Ter-Akopyan, and A. V. Yeremin, Z. Phys. A **345**, 389 (1993).
[3] T. Sikkeland, A. Ghiorso, and M. J. Nurmia, Phys. Rev. **172**, 1232 (1968).
[4] E. A. Cherepanov, A. S. Iljinov, and M. V. Mebel, J. Phys. G **9**, 1397 (1983).
[5] W. Loveland, Nuclear Chemistry Progress Report, Oregon State University, August 2000 (unpublished).
[6] K. E. Rehm, Annu. Rev. Nucl. Part. Sci. **41**, 429 (1991).
[7] P. Armbruster, Annu. Rev. Nucl. Part. Sci. **50**, 411 (2000).
[8] S. Bjornholm and W. J. Swiatecki, Nucl. Phys. **A391**, 471 (1982).
[9] A. V. Ignatyuk, G. N. Smirenkin, and A. S. Tishin, Yad. Fiz. **21**, 485 (1975).
[10] L. G. Moretto, Nucl. Phys. **A182**, 641 (1972).
[11] D. J. Hinde, R. du Rietz, M. Dasgupta, R. G. Thomas, and L. R. Gasques, Phys. Rev. Lett. **101**, 092701 (2008).
[12] A. Samant and S. Kailas, Z. Phys. A **356**, 309 (1996).
[13] M. G. Itkis *et al.*, Nucl. Phys. **A787**, 150c (2007).
[14] Y. Aritomo, M. Ohta, and F. Hanappe, J. Phys. G: Nucl. Part. Phys. G **32**, 2245 (2006).
[15] G. N. Harding and F. J. M. Farley, Proc. Phys. Soc. London Sect. A **69**, 853 (1956).
[16] A. Gavron *et al.*, Phys. Rev. C **35**, 579 (1987); D. J. Hinde, D. Hilscher, H. Rossner, B. Gebauer, M. Lehmann, and M. Wilpert, *ibid.* **45**, 1229 (1992); D. Hilscher, I. I. Gontchar, and H. Rossner, Yad. Fiz. **57**, 1255 (1994).
[17] H. H. Knittner, U. Brosa, and C. B. Jorgenson, in *The Nuclear Fission Process,* edited by C. Wagemans (CRC, Boca Raton, Fla., 1991).
[18] E. Holub *et al.*, Phys. Rev. C **33**, 143 (1986).
[19] W. Reisdorf, Z. Phys. A **300**, 227 (1981).
[20] W. Reisdorf and M. Schadel, Z. Phys. A **343**, 47 (1992).
[21] O. Batenkov *et al.*, Nucl. Instrum. Methods Phys. Res. A **394**, 235 (1997).
[22] C. Rouki, Ph.D. thesis, Uppsala University, 2004.
[23] K. Elmgren, Ph.D. thesis, Uppsala University, 2002.
[24] W. Mannhart, IAEA Tecdoc-410, 158, 1986 (unpublished).
[25] H. W. Schmitt, W. E. Kiker, and C. W. Williams, Phys. Rev. **137**, B837 (1965).
[26] Y. A Lazarev, O. K. Nefediev, Y. T. Oganessian, and M. Dakowski, Phys. Lett. **B52**, 321 (1974).
[27] C. J. Bishop, I. Halpern, R. W. Shaw, Jr., and R. Vandenbosch, Nucl. Phys. **A198**, 161 (1972).
[28] D. Peterson, W. Loveland, O. Batenkov, M. Majorov, A. Veshikov, K. Aleklett, and C. Rouki, AIP Conf. Proc. **610**, 613 (2002).
[29] A. N. Andreyev *et al.*, Dubna report E7-94-378, 1994 (unpublished).
[30] M. H. Simbel, Z. Phys. A **313**, 311 (1983).
[31] R. Vandenbosch and J. R. Huizenga, *Nuclear Fission* (Academic, New York, 1973), p. 323.
[32] P. Moller, J. R. Nix, W. D. Myers, and W. J. Swiatecki, At. Data Nucl. Data Tables **59**, 185 (1995).
[33] W. D. Myers and W. J. Swiatecki, Phys. Rev. C **60**, 014606 (1999).

[34] A. Ignatyuk *et al.*, Sov. J. Nucl. Phys. **21**, 612 (1975).
[35] W. J. Swiatecki, K. Siwek-Wilczynska, and J. Wilczynski, Acta Phys. Pol. B **38**, 1565 (2007).
[36] G. Audi, A. H. Wapstra, and C. Thibault, Nucl. Phys. **A729**, 337 (2003).
[37] S. Cwiok, Z. Lojewski, and V. V. Pashkevich, Nucl. Phys. **A444**, 1 (1985).
[38] M. Duijvestijn, A. Koning, and F. J. Hambsch, J. Nucl. Sci. Technol. Supp. **2**, 754 (2002).
[39] O. A. P. Tavares and E. I. Medeiros, J. Phys. G: Nucl. Part. Phys. **30**, 395 (2004).
[40] A. D'Arrigo, G. Giardina, M. Herman, A. V. Ignatyuk, and A. Taccone, J. Phys. G: Nucl. Part. Phys. **20**, 365 (1994).
[41] K. Pomorski, B. Nerlo-Pomorska, and J. Bartel, Int. J. Mod. Phys. E **16**, 566 (2007).
[42] H. A. Kramers, Physica (Utrecht) **7**, 284 (1940).
[43] V. I. Zagrebaev, Y. Aritomo, M. G. Itkis, Y. T. Oganessian, and M. Ohta, Phys. Rev. C **65**, 014607 (2001).
[44] V. M. Strutinsky, Phys. Lett. **B47**, 121 (1973).
[45] P. Grange and H. A. Weidenmuller, Phys. Lett. **B96**, 26 (1980).
[46] P. Grange, Li Jun-Qing, and H. A. Weidenmuller, Phys. Rev. C **27**, 2063 (1983).